AD-A079 285 FLORIDA STATE UNIV TALLAHASSEE DEPT OF OCEANOGRAPHY F/G 8/3
SURFACE METEOROLOGY OVER THE GATE A-SCALE.(U)
NOV 78 T N KRISHNAMURTI, R KRISHNAMURTI N00014-75-C-0877
UNCLASSIFIED 78-6 NL

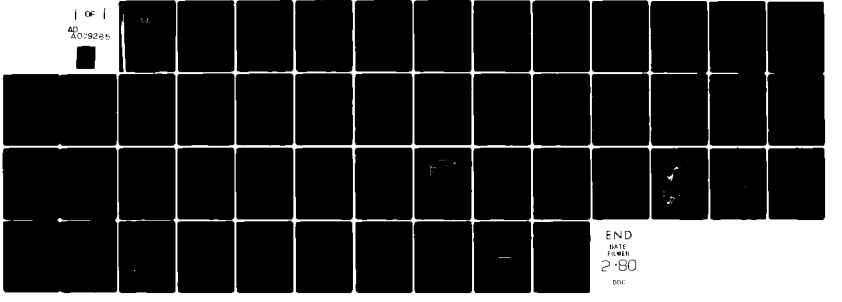

SURFACE METEOROLOGY OVER THE GATE A-SCALE

(12)

LEVEL II

BY
T. N. KRISHNAMURTI
AND
RUBY KRISHNAMURTI

DEPARTMENT OF METEOROLOGY
AND OCEANOGRAPHY
FLORIDA STATE UNIVERSITY
TALLAHASSEE, FLORIDA 32306

Supported by
NSF Grant No. ATM75-18945
and
ONR N-00014-75-C-0877

Report No. 78-6

SURFACE METEOROLOGY OVER THE GATE A-SCALE

BY

T. N. KRISHNAMURTI*

AND

RUBY KRISHNAMURTI*

DEPARTMENT OF METEOROLOGY*
AND OCEANOGRAPHY*
FLORIDA STATE UNIVERSITY
TALLAHASSEE, FLORIDA 32306

Abstract

A method of analysis for the surface motion field based on a mix of observations from research ships, merchant ships and low cloud motion vectors from geostationary satellites is proposed in this paper. The proposed scheme permits a turning of wind with height between the cloud wind level and the surface. This turning is incorporated via a successive correction procedure which enables us to fully utilize the low-cloud winds. The method does not depend on the selection of a level of best fit for the cloud winds and thus is not dependent on a predetermined theory. The analysis of the surface wind field is carried out for the 100 days of the GARP Atlantic Tropical Experiment (GATE) for two observation periods per day (00Z, 12Z) over a wide domain.

This paper illustrates i) time averaged geometry of the motion field during GATE, and ii) time averaged fields of the zonal and the meridional stresses as well of the curl of the wind stress. Finally, we examine the spectral analysis of the motion field and the stresses over the trade wind belts of the summer and winter hemisphere. Our study emphasizes the importance of two modes of oscillation, one around 3 to 6 days and the other around 10 to 15 days. While the former is identified with African waves, the scale and speed of propagation of the latter is determined from x-t diagrams and is identified as a westward propagating wave, whose scale is of the order of 40^{o} longitude and speed of propagation is around 3^{o} longitude/day. This study emphasizes the possible usefulness of this approach during the GARP Global Experiment when a global coverage from geostationary satellites is expected.

1. Introduction

In this paper we propose a new method for describing the surface motion field over the oceans from a mix of observing systems such as: research ships, merchant ships and cloud winds from geostationary satellites. The purpose of this exercise is to define the values of surface stresses over certain space and time scales for investigations of air-sea interactions. The period of the GARP Atlantic Tropical Experiment (GATE) provides us with a unique data set to carry out these investigations in somewhat greater detail than has been possible previously.

The definition of a surface motion field over the GATE oceans is of considerable interest to oceanographers. Problems such as equatorial oceanography, the Guinea coast upwelling and the Gulf of Mexico water circulations can be examined with the composite GATE surface meteorological data sets.

The present study focuses on an analysis technique that enables us to bring the cloud winds (low cloud motion vectors) to the sea level with an allowance for the turning of the wind with height. This turning of wind with height is determined here without relying on any specific theory of the planetary boundary layer. The procedure relies on an updating of the wind shear between the cloud wind level and the surface level via a successive correction of an objective analysis at the two levels with the available data sets.

In Section 2 of this paper, we shall present a list of data sources available for this study. Section 3 provides details on the proposed analysis method. In Section 4 we show sample GATE mean maps as well as sample analyses for individual days. The mean fields of the surface stresses and the

curl of the surface wind stress are illustrated in Section 5, and the salient time variability of the relevant parameters are presented in Section 6.

2. Data Sources

Fig. (1) illustrates the configuration of GATE ships during one phase of the Experiment. There were roughly 30 research ships that provided surface meteorological observations during the three phases of GATE (roughly 8 weeks per phase). This data set was prepared by the Synoptic Scale Subprogram Data Center at Bracknell. In this study we have used the 00Z and 12Z data sets from roughly 25 ships during the three phases.

The marine data collection from merchant ships comes from two sources: 1) The Global Telecommunication Service tapes, and ii) the Marine data tapes from the Weather Service of the Federal Republic of Germany. The latter was special collection for GATE. Roughly 1400 ship observations per 24 hour day were available during the 100 days of GATE from these sources. For one maptime (e.g., 00Z $\pm$ 6 hours) a typical distribution of this data set is illustrated in Fig. 2. The quality of this data requires a stringent screening, which is carried out in the analysis phase described in the next section.

The cloud motion vectors described in the present study were collected (as well as processed) by Krishnamurti et al (1976a). This data set includes cloud winds from two geostationary satellites, ATS III and SMS 1. During a 24 hour period roughly 1400 low cloud motion vectors were collected for the 100 days. Fig. (3) (from an unpublished study of Fujita) illustrates a possible maximum data coverage over the Atlantic ocean from a geostationary satellite.

Among these data sets the accuracy of the GATE ship data is thought to be of the order of 2 mps for speed and 10° for direction. The corresponding figures for the cloud winds applied to 850 mbs is of the order of 4 mps and 20° respectively, (Hubert , 1975). It is not possible to assess the quality of the merchant ships in a similar manner. However, it is our contention that if this voluminous data is subjected to a screening via elimination of those observations whose standard deviation with respect to a local mean exceeds the same limits as the accuracy of the cloud winds, then the retained data set becomes extremely valuable.

3. Method of Analysis

3.1 The Background

The basic approach for data analysis of the wind velocity components (u and v) is a successive correction method proposed by Cressman (1959). This method is quite suitable for handling such fields if there is an adequate coverage and if the data from a diverse set of platforms is adequately handled. For low latitude analysis of the above fields it is felt that a man-machine mix (i.e., insertion of bogus data) is useful in order to introduce continuity in sparse data areas: roughly 6 such data insertions per maptime within a total of 300 to 400 observations per day were made. This amounts to roughly 2% of such bogus data for the 100 days of GATE. Roughly one bogus data per day was introduced in southwestern Pacific ocean (100°N, 10°S) equatorial region near 40°N, North African desert regions (5°N, 20°N) and South Central Atlantic ocean near 15°N and 12°S. We feel that this exercise has been extremely useful in providing us with very useful fields of surface parameters. In the absence of such bogus data, there is a tendency for the motion field to exhibit fictitious asymptotes of convergence or shear lines

in the interfacial region between data rich areas and those defined via the first guess field.

The details of the objective analysis scheme, used here, is discussed in Tripoli and Krishnamurti (1975) and hence it will not be reviewed in detail here. The domain of analysis extends from 20^{O}S to 34^{O}N and 100^{O}N to 14^{O}E. We use a 2^{O} latitude by 2^{O} longitude grid in our analysis. The mean separation distance between observations, D, is of the order of 350 km. The influence radius, R, is decreased in successive correction scans starting from 5xD to 2xD in the final scan.

The objective analysis scheme has a data rejection cycle which works as follows: We allow four successive scans in the analysis. During each scan, ν , the error is given by the relation

$$E_s^{\nu} = u_s^{\nu} - u_{gs}^{\nu} \qquad (1)$$

where u_s^{ν} denotes a wind component at an observation site, while u_{gs}^{ν} denote the interpolated value at that point. The successive scans, as shown in Tripoli and Krishnamurti (1975), reduce the magnitude of E_s^{ν} . Data rejection criteria are based on the magnitudes of E_s^{ν} for each scan, ν (Yanai , 1964). In this study we define these limits = 12, 10, 8, and 6 mps for the successive scans. Both components of the wind (u and v) were independently handled with the same rejection criteria. A prescreening of the data sets includes a limit on the maximum surface winds and procedure for the removal of duplicate data.

The maximum surface wind on our resolution is 30 mps. Any wind greater than that value is rejected by the analysis technique. A data set program removes all duplicate data in the first scan. The first guess field for the wind analysis for the first day (i.e., June 16, 1974 00Z) is prepared

on the basis of subjective analysis of the same data. Thereafter persistence is used to define a first guess field. It should be stated that since the final data set includes around 400 observations, the first guess is not very critical for the final analysis.

The first step in this exercise is to apply the above method and perform an objective analysis at the surface and the 850 mb level. This surface analysis utilizes surface marine, GATE and the World Weather Watch Surface Network data within the domain. No cloud winds enter the surface analysis at this stage. This procedure is carried out for every 12 hours for the 100 days of GATE. Except for the first maptime all the remaining analysis utilize 'persistence' (i.e., 12 hour earlier field) as a first guess field in the objective analysis. Because of the large amounts of observations per maptime, (00Z or 12Z) $\pm$ 6 hours, the first guess is not retained over most regions.

The 850 mb level analysis utilizes all available types of observations: Radiosonde/rawinsonde, pilot balloon, research aircraft low resolution data and low cloud motion vectors. The method of analysis of this data set is described in Tripoli and Krishnamurti (1975). The motion field was analyzed for 00Z and 12Z for the 200 maptimes.

The next step in this exercise is to determine a mean turning angle of the wind based on the above stated first guess fields: low cloud motion vectors are generally used in the analysis of the cloud base level charts, i.e. roughly 1 km above the sea level. Since a sizeable turning of wind with height ($\simeq$ 20°) occurs in this depth (Brummer et al,1973; Holland and Rasmussen, 1973; Charnok et al., 1956) it seems inappropriate to use the cloud winds directly at the surface level. There is no simple analytical

method for accounting for the turning of the wind with height. We have arrived at an empirical method for incorporating the cloud wind data to the surface level by a method of successive corrections that takes into account the mean turning of the winds with height in 12 subregions (called sections here) over the oceanic regions.

3.2 Mean Turning Angle Within a Sector

Within one of these sections, at grid point i,j, the surface and the cloud level wind directions may respectively be written as: (the symbols are explained in Table 1).

$$D_{s,ij} = \tan^{-1} \left(V_{s,ij} / u_{s,ij} \right) \quad (2)$$

and

$$D_{c,ij} = \tan^{-1} \left(V_{c,ij} / u_{c,ij} \right) . \quad (3)$$

The turning angle may be written as: $\delta_{ij} = D_{s,ij} - D_{c,ij} .$ (4)

The mean turning angle is obtained by summing δ_{ij} over all the grid points within the subdomain,

$$\bar{\delta} = \sum_j \sum_i \left\{ \tan^{-1} V_{s,ij}/u_{s,ij} - \tan^{-1} V_{c,ij}/u_{c,ij} \right\} / N \quad (5)$$

where N denotes the number of points within the subdomain. The speed of the surface and the cloud level winds at point i,j is given by the respective relations:

$$S_{s,ij} = \sqrt{u_{s,ij}^2 + V_{s,ij}^2} \quad (6)$$

$$S_{c,ij} = \sqrt{u_{c,ij}^2 + V_{c,ij}^2} \quad (7)$$

The mean wind speed for the subdomain for the surface and the cloud levels respectively is next obtained by a summation of the speeds,

$$\bar{S}_s = \sum_j \sum_i S_{s,ij} / N \quad (8)$$

$$\bar{S}_c = \sum_j \sum_i S_{c,ij} / N . \quad (9)$$

The individual cloud wind observations (S_c , D_c) within the subdomain are next relocated at the surface level via the relations:

$$u_{cs} = S_c \{ \cos (D_c + \bar{\delta}) \} \bar{S}_s / \bar{S}_c \quad (10)$$

$$v_{cs} = S_c \{ \sin (D_c + \bar{\delta}) \} \bar{S}_s / \bar{S}_c . \quad (11)$$

The aforementioned analysis is not constrained to a precise knowledge of the height of the cloud winds. The analysis is independent of this height. Although we assigned the cloud winds to the 850 mbs, the final results over oceans would have been the same if we had assigned a different height to the low cloud motion vectors provided the upper level is analyzed using only the cloud wind observations. The emperical approach proposed here is not constrained by any boundary layer theory and as such is not limited to a barotropic or a baroclinic theory in the near equatorial latitudes. The following analysis shows the validity of the proposed method if the boundary layer were barotropic:

We start with a logarithmic profile for the variation of wind with height:

$$u_g/u_* = 1/k \ln z_a/z_0 \quad (12)$$

where k is the Von Karman constant and Z_0 is surface roughness.

Following Wyngaard (1975) we introduce

$$z_a = -CL \quad (13)$$

where L is the Monin Obukhoff length and C is the constant. Thus we obtain

$$u_g/u_* = 1/k \ln -L/z_0 + 1/k \ln C . \quad (14)$$

We omit the second term, which is negligible, and thus obtain

$$k u_{go}/u_* = \ln (-L/z_0) . \quad (15)$$

Similarly we obtain

$$- k V_{g0}/u_* = k u_*/fh \qquad (16)$$

where the height of the planetary boundary layer h may be equated to the cloud base level for convenience.

Next we define,

$$\tan \alpha_0 = V_{g0}/u_{g0} \qquad (17)$$

where α_0 is the angle between the surface wind (along the x axis) and the pressure gradient force (i.e., the cloud wind direction for a barotropic boundary layer).

Substituting for V_{g0} and u_{g0} we obtain,

$$\tan \alpha_0 = - \frac{k \{ u_*/fh \}}{\ln \{ -L/z_0 \}} \qquad (18)$$

hence

$$\alpha_0 = \tan^{-1} \left\{ \frac{-k (u_*/fh)}{\ln (-L/z_0)} \right\} \qquad (19)$$

Thus $\alpha_0 = f(z_0, L)$ (a function of z_0 and L), and $-k \frac{u_*}{fh}$ may be assumed to be a constant $\simeq -0.1$.

If θ_0 is the angle between the pressure gradient (i.e., the cloud wind) and the east, then we may write:

$$\alpha_0 + \theta_0 = F(z_0, L) + \theta_0 \qquad (20)$$

This expression is consistent with our empirical expression presented above. Thus, at least for a barotropic boundary layer our empirical method for the turning of the cloud wind with height can be rationalized. Since the sub-domains of the analysis are fairly small, we believe that our analysis is also valid for baroclinic situations.

3.3 Steps in the Analysis Procedure

i) Analyze surface streamlines and isotachs using only GATE and merchant ships data sets.

ii) Finalize the 850 mb analysis of the motion field using a mix of observations from radiosonde/rawinsondes, pilot balloons and low cloud motion vectors (Tripoli and Krishnamurti, 1975).

iii) Determine the sector mean turning angle and the mean wind shear.

iv) Relocate low cloud motion vectors at the surface level and modify their speeds and directions by the turning angle and speed ratios determined in step iii).

v) Reanalyze the surface charts using modified cloud winds, World Weather Watch surface data, GATE and merchant ship data. Use the previous surface analysis to provide a first guess field.

vi) Repeat steps iii), iv) and v) until surface analysis converges, i.e. the speeds and directions of the two successive scans of step v) at a grid point do not alter by more than 2 mps and 2^{O} respectively for successive scans.

3.4 On the Validity of the Analysis Scheme

Three types of tests were carried out to investigate the validity of the proposed analysis of the motion field over the oceans.

i) Comparison with an independent analysis of the phase mean motion field: Our time averaged motion field for phase III of GATE (12Z data only) was intercompared with a corresponding subjective analysis (Dean and Smith , 1977), Based on GATE ships plus a smaller collection of the marine data, the two analyses illustrated in Figures 4a and 4b are in essential

agreement within the regions $5^{o}S$ to $15^{o}N$ and $40^{o}W$ to $15^{o}W$. The direction and locations of the north-east and the south-east trade winds, the West African monsoons, the flow separation point near $9^{o}N$, $34^{o}W$, and the asymptote of convergence are in close agreement. The speed field over certain areas such as $20^{o}W$ and $3^{o}N$ exhibit differences and we feel that this discrepancy is largely due to a total lack of observations in the analysis of Dean and Smith (1977). It should be noted that our analysis utilizes more observations from the diverse observing system over the domain. In regions where comparable observations of high quality are available such as over the GATE A/B scale ship array, the two analyses show close agreement in both wind direction and speed.

ii) Comparisons of sample daily surface motion field from the Dean and Smith (1977) subjective analysis and our objective analysis show some minor discrepancies. The differences are again related to the disparity in the number of observations over the large data void regions in the analysis of Dean and Smith (1977). The two analyses tend to be in close agreement over the regions of the A/B scale ship network. Fig. (4c) illustrates a typical surface chart for a single day. The analysis illustrates a disturbance on the 6th of September, 1974 (00Z) over the GATE A/B scale, as well as hurricane Carmen in the southern Gulf of Mexico. The details of these flow fields show a very reasonable interdiurnal time continuity.

iii) An intercomparison of observed surface ship data with an interpolation of our analysis to these locations shows that our winds are an underestimated by about 10% (e.g. 4 mps instead of 4.5 mps). This is due to the fact that the objective analysis scheme provides a grid point wind which is in fact a mean over a domain whose size $\simeq 200\ km^2$. Thus some

of the episodes of large fluctuations of wind within the A/B scale array do not agree with the point values represented by the ship data. This discrepancy will also be reflected in the magnitude of the stresses as well as in the estimates of the curl of the wind stresses. Furthermore, since the latter are proportional to the square of the wind speed, they will thus reflect a further enhancement of this discrepancy. It is however important to recognize that the proposed objective analysis, with an influence radius 100 km, will give an areal average representation of the motion field and the stresses on this scale. There is no essential difference between results based on our analysis and those obtained from a direct use of GATE ship observations, if we recognize that the former represents an areal average while the latter denotes values at single locations.

4. Mean Motion Field During GATE

4.1 Surface and 850 Mb Fields

In figures (5a, b) we illustrate the mean surface wind field for the 100 days and the third phase of GATE respectively. The averages here are based on the final daily analysis at 00Z as well as at 12Z. The surface flows show a well defined African monsoonal flow over West Africa which penetrates well inland. The northeast trades over the Atlantic Ocean have a mean speed of around 10 to 15 knots. The southeast trades of the eastern Pacific Ocean exhibit a distinct turning toward the east as the flows cross the equator. The location of the surface asymptote of convergence is consistent with the location of the ITCZ based on cloud cover (M. Murakami, 1979). The southeast trades of the Atlantic Ocean

have an interesting source region at the southern boundary of the analysis roughly between $5^{o}S$ and $14^{o}E$. This flow has essentially two branches: i) the monsoonal branch that eventually acquires a westerly component, and ii) the easterly branch that flows toward South America.

Fig. (6a, b) illustrates the time averaged motion field at 850 mbs for the 100 days and phase III of GATE. At this level the trade winds have an intensity between 15 and 20 knots over the Atlantic and eastern Pacific oceans. The southeast trades show the strongest speeds over northeastern Brazil. The southwesterly flows over West Africa do not penetrate north of $15^{o}N$ at this level.

Compared to the 100 day average the third phase of GATE shows stronger trade winds over the northeastern Atlantic ocean, as well as over the central Atlantic Ocean in the Southern Hemisphere.

These fields over oceans are largely determined by the cloud motion vectors. Of major interest here is the difference between the surface level and the 850 mb flows.

4.2 The Field of the Mean Turning Angle

From the final analysis at the surface level and at the level of the low cloud winds we have constructed a 100 day mean chart of the 'mean turning angle' between these two levels. The turning angle (Fig. 7) is extremely large along the West African, South American and the Central American coasts over the eastern oceans. In these regions the surface westerly winds change to easterlies at the cloud wind level. Cloud drifts in low latitudes are almost always from east to west.

A word of caution in interpretation is necessary here. The cloud-wind level should not be tacitly assumed to be the top of the friction layer. It is conceivable that shallow clouds may in fact be found within

the friction layer. Hence, the turning angle described may not be the total turning of the wind in the lowest layer.

By and large the southeast trades of the Atlantic and eastern Pacific ocean show backing of wind with height while the northeast trades exhibits a veering. The angle of backing (or veering) in the trade wind belts is on the order of 8^{o} to 16^{o} between the surface and the cloud drift level. In the transition zones such as the vicinity of the ITCZ the turning angle can be as large as 180^{o} because of a complete reversal of wind direction.

5. Time Averages of the Wind Stress and the Curl of the Wind Stress

5.1 The Drag Coefficient

During GATE, the buoy observations from the ship 'METEOR' were used to estimate momentum fluxes by the eddy correlation method (Dittmer et al, 1978). From a comparison of their results with those obtained using the Bulk Aerodynamic Method, Pusinger and Seguin (1977) recommended that the drag coefficient (C_D) for undisturbed as well as disturbed conditions lies in the range $1.4 \pm 0.4 \times 10^{-3}$. We feel that for large scale flows (i.e. on the GATE A-scale) this is certainly an appropriate choice. However, noting the fact that there were several hurricanes during the 100 days within the GATE A-scale domain, we feel that a variation of drag coefficient with wind speed is appropriate for the mapping of the stress charts. Angular momentum budget studies in tropical disturbances clearly show that the drag coefficient does vary with the radial distance from the center of the hurricane as well as with respect to the wind speed in a

hurricane (Miller, 1962, Ooyama, 1969). During GATE on the A-scale, our tabulation on the 2^{o} latitude/2^{o} longitude mesh size does not resolve the fine structure of the high speed region (the inner rain area) of a hurricane. However we note occasional wind speeds as large as 45 knots during such events. Thus, following Roll (1965) and Miller (1962), we estimate the stresses for wind speeds 10 mps by using the formula

$$\begin{matrix}\tau_x \\ \tau_y\end{matrix} = C_D \rho \begin{matrix}u \\ v\end{matrix} \sqrt{u^2+v^2}\ , \quad C_D = 1.4 \times 10^{-3}.$$

Wind speeds $>$ 10 mps are estimated by using

$$\text{and} \quad \begin{matrix}\tau_x \\ \tau_y\end{matrix} = C_D \rho \begin{matrix}u \\ v\end{matrix} \sqrt{u^2+v^2}\ , \quad C_D = 0.7 + 0.07|V| \text{ for wind speeds } > 10 \text{ mps.}$$

This is consistent with the value of 1.4×10^{-3}, for a wind speed of 10 mps suggested by Businger and Sequin (1977). It also gives reliable estimates at high wind speeds. The choice of a constant drag coefficient for speeds less than 10 mps is also suggested by the results from 'BOMEX' observations.

5.2 The Curl of the Wind Stress (CWS)

Holopainen (1967), Hantel (1970) and Duing (1968) have examined the distribution of CWS over wide areas from long-term time-dependent motion fields. Hantel and Duing examined the Indian Ocean region in considerable detail and noted large zonal gradients of the wind stress curl in the southwesterly monsoonal current. Hantel's charts clearly bring out a relationship between the wind stress curl and the observed regions of cold upwelling in the western Arabian Sea. They also noted that the surface winds in the Indian Ocean were quite large, and as a consequence, stresses of the order of 1 dyne/cm^2 and curl of wind stress of the order of 2.5×10^{-8} dynes/cm^3 were noted in their calculations. Hantel used a drag coefficient of 1.2×10^{-3} which is closer to the value

we have used in the present study for the GATE A-scale region.

We examined the GATE phase mean and 100 day mean distribution of the wind stress curl defined by the relation,

$$C_{ws} = \frac{\partial \tau_y}{\partial x} - \frac{\partial \tau_x}{\partial y}$$

The fields were computed by straightforward centered differences over a distance of Δx and Δy on the order of 200 kms.

Aside from the time averaged fields we shall also show the variability and time spectra of CWS in this section. The resolution of the data (two maps per day) limits the scope of this study. It should be noted very clearly that the smallest resolvable wave in the present context is $\simeq$ 400 kms in space and two days in time. Furthermore, since only oceanic and near coastal data are used for the analysis of the wind stress curl over the oceanic domain of the GATE A-scale, the near coastal analyses within a few hundred kms are not too reliable. This limits the usefulness of the presented data sets for studies of coastal oceanographic problems of local origin.

5.3 The Time Averaged Wind Stress and the Wind Stress Curl

Figs. (8a, b) respectively illustrate the 100 day and the Phase III mean meridional wind stress distribution over the GATE A-scale oceans. In Fig. (8a) the zero line in the middle of the Atlantic Ocean separates a northerly meridional shear to its north from the southerly shear to its south. The magnitude of the shear is largest near the North African coast and the Eastern part of the southern Atlantic Ocean. The southeast trades exert a stronger meridional stress than the northeast trades over the

tropical Atlantic Ocean. The magnitude of the meridional stresses over the trade wind belt varies from 1.0 to 1.25 dynes/cm^2 (Note: 1 dyne/cm^2= 0.1 N/m^2). The estimates for phase III are slightly larger than those for the 100 day mean. Over the Eastern Pacific Ocean near the Peruvian coast, the magnitude of the meridional stresses show two maxima, which are especially strong ($\simeq$ 2 dynes/cm^2) during the third phase of GATE. This region has an abundant distribution of cloud winds. A zero line separates the positive and negative stresses over the western part of the Gulf of Mexico. The northern part of the western Gulf exhibits west south-westerly flows while the southern part of the Gulf shows west north-westerly flows. The corresponding meridional stresses in the western Gulf are on the order of 0.5 dynes/cm^2.

The zonal stress for the 100 days and the third phase is illustrated in Figs. (9a, b). It is stronger over the central Atlantic Ocean, reaching magnitudes in excess of 1.5 dynes/cm^2. The summer hemisphere trades exerts a stronger zonal stress while the winter hemisphere trades have a stronger meridional stress over the Atlantic Ocean. Over most of the tropics the stress is from the easterly direction, except for the monsoonal belt near the eastern Atlantic and Pacific oceans. Both the zonal stress and the meridional stress show a relative maximum value between 0° and 10°E and south of 15°S. This appears to be a source region for surges in the velocity of southeast trades of the southern Atlantic Ocean. In general, the magnitude of the zonal stress is roughly 15% greater during the third phase compared to the 100 day mean.

The field of the total stress is illustrated in Fig. (10a, b) for the 100 days and the third phase respectively. The total stress is larger in the northeast trades in comparison to the southeast trades. The maximum value

exceeds 2 dynes/cm^2. The mean value of the total stress for the 100 days over the GATE A/B scale is around 0.3 dynes/cm^2. This is slightly smaller than the magnitudes of 0.4 dynes/cm^2 reported by Jacobs (1978). The reasons for this discrepancy are discussed elsewhere in this paper. The regions along the Peruvian coast, along the western Gulf of Mexico, around 10^{o}N and 100^{o}W and around 20^{o}S and 5^{o}E are other regions with large stresses. It is of interest to compare the magnitudes of the stresses estimated here with earlier estimates given by Hellerman (1967).

Hellerman's (1967) well known seasonal mean tabulations of wind stresses (τ_x and τ_y) were based on U.S. Navy Hydrographic Offices' Marine Climatic Atlas of the World. This atlas was based on roughly 8 years of marine surface data. Fig. (11a and b) show Hellerman's mean fields of the wind stresses τ_x and τ_y for the summer months (June, July and August). Although there is a general agreement between our analysis, Fig. (10a, b) during GATE (Mean Stresses for the period June 16 through September 23rd), there are some major differences as well:

a) Zonal stresses: In the northern trade wind belt our analysis shows a belt of easterly zonal stress around roughly 20^{o}N. The corresponding latitude of strongest zonal easterly stress in Hellerman's study is located closer to the equator (17.5^{o}N to 7.5^{o}N). The trade belt of strongest winds during GATE seems to be located somewhat farther north. The strongest magnitude of the stress in Hellerman's tabulations are around 1 to 1.4 dynes/cm^2 while those shown in the present study are around 1.6 dynes/cm^2. The major difference is due to differences in the intensity of the trades. For steady trade wind speeds on the order of 10 mps, we have used a drag coefficient of 1.4 x 10^{-3} based on recent GATE

summaries presented by Businger and Seguin (1977). Hellerman used a value of 2.6×10^{-3} for those same wind speeds. It should also be noted that we have used daily values of the wind in estimating our mean stresses, while those of Hellerman's study are based on long term mean motion field and wind roses that contain some information on the frequency distribution of daily stresses.

b) Meridional stresses: In the region of the northeast trades, the meridional stress is largest around 17.5°N to 7.5°N in the tabulations of Hellerman, while our study shows that the strongest trades are, in fact, found farther north and closer to 20°N. This is primarily due to the differences in the mean motion fields of our study versus those found in the U.S. Hydrographic Marine Climatic Data Summary. The southern trades exhibit winds greater than 10 mps over a wide region of southeastern Atlantic Ocean. The use of a drag coefficient of 2.6×10^{-3} in Hellerman's tabulations again leads to rather large magnitudes of the meridional stresses. In this region the magnitude of largest meridional stress in Hellerman's study is on the order of 0.5 dynes/cm^2, while in our study it is somewhat larger inspite of our use of much smaller drag coefficients due to stronger winds and transients. Details of stresses within the Gulf of Mexico and in the eastern Pacific ocean are not described by the climatological data set of Hellerman.

Finally, we shall examine the mean fields of wind stress curl for the 100 days and the third phase of GATE, Fig. (12a, b). The trade wind belts contain an east-west oriented zero line separating regions of negative and positive wind stress curl. In the northern trades this separation

line is located around 20°N, and for the southern trades this line is located along 10°S. In general, a positive and an adjacent negative center is found over most regions of strong wind stress curl. The positive center is to the left of the strong wind stress vector while the negative center is to its right. Such couplets are clearly evident in the western Gulf of Mexico, the Caribbean Sea, the Eastern Pacific Ocean, the northeast trades (20°N) and the southeast trades over the eastern Atlantic Ocean. The Guinea coast is a region of some interest here. The only region with a positive wind stress curl along this coast is located near 3°E where a meandering of the zero line may be noted. Over most of the remaining regions along this coast, the wind stress curl does not show positive values north of the equator. This situation is quite different from that along the Peruvian coast. The winds along the Peruvian coast contain a stronger southerly coastal flow, while in the southern Atlantic ocean stronger south westerlies are found and the flows parallel to the African coast are not as large.

6. Spectral Analysis of GATE Surface Fields

In this section we shall present a spectral analysis of some of the surface parameters of the present study. The first step in this analysis is the removal of root mean square linear trend since there may be present some seasonal changes on the scale of the 100 day period. We note from plots of data that the seasonal trend is indeed quasilinear and hence the linear regression is found quite adequate for the surface parameters during the summer season. Our numerical method is the direct fast Fourier transform method of spectral analysis. In the execution of the spectral

analysis we follow the earlier works of Wallace (1971), Yanai et al (1968), Zangvil (1975) and Krishnamurti and Bhalme (1976b).

The coefficient of an $\{X\}$ series is given by:

$$X_k = \sum_{j=0}^{N-1} x_j e^{i2\pi k} \; ; \; k = 0, 1, 2, \ldots N-1. \qquad (21)$$

where x_j represents the data points and N the number of coefficients. The power spectral estimates of the series are given by,

$$G_{xk} = 2\Delta t/N \; |X_k|^2 \; ; \; k = 0, 1, 2, \ldots N-1. \qquad (22)$$

where Δt is the time interval. Smoothed estimates may be obtained by averaging L contiguous raw estimates to yield,

$$G_{xk} = L^{-1} \sum_{j=1}^{L} G_{x(k+j)} \qquad (23)$$

Our present interest will be first to examine the power spectral density over some of the key regions of interest in the GATE A-scale. For purposes of depiction we shall illustrate the product of the power (per cent variance) times the frequency (along ordinate) versus the log of the frequency (along abscissa). The advantages of this representation have been enumerated by Zangvil (1975).

6.1 Northeast trades (Atlantic Ocean)

The variability is here described for a rectangular region, 2000 km x 1000 km, centered at 40°W and 20°N. The zonal wind (see Fig. 13a) in this region is around 5 mps with peak values close to 11 mps. During the 100 days the easterly zonal velocity of the northeast trades shows several peak

velocity periods roughly 15 days apart with evidence of some variability on shorter time scales. The spectral analysis of the zonal wind is illustrated in Fig. 13b. This shows a dominant oscillation of around 15 days. There is also considerable power in shorter time scales of less than 10 days. A peak of around 30 days is not very reliable due to the fact that the length of the data records is only 100 days.

The spectra of the meridional velocity (Fig. 14a) in this region of the northeast trades show a dominant mode of around 5 days with shorter time scales of 2 to 5 days. The meridional velocity also exhibits a pronounced oscillation in the 10 to 15 day time scales. Finally, we present the spectra of the total wind stress for the Northeast trades in Fig. 14b. This exhibits a most pronounced peak around 11 and 17 days as well as some variability between 2 to 6 days.

6.2 Southeast Trades (Atlantic Ocean, Centered at Equator and 30°W)

The corresponding illustrations are the variability of the zonal wind during the 100 days, and its spectra are respectively shown in Figs. 15a, b. The zonal wind shows considerable variability around 3 days and 10 to 15 days. This variability of surface zonal wind in the Southern as well as the Northern Hemisphere is consistent with the findings of Krishnamurti et al (1975) from the cloud winds during GATE. In this study an oscillation in the intensity of the trades with a period of around 14 days was described. Furthermore, a near simultaneous occurrence of surges in the trades of the two hemispheres was noted in the GATE 'Cloud Wind' data sets. A careful superpositioning of Fig. 13a on top of Fig. 15a shows that an interesting relationship exists between the trades of the two hemispheres

at the surface level as well. During the first half of GATE the maxima in the Northeast trades seem to follow the maxima of the trade winds of the Southern Hemisphere with a lag of roughly 3 days. After the first part of August, 1974 with the advent of the active phase of African disturbances, the maxima of the Northern trades appear to precede the corresponding maxima of the Southern trades. A careful examination of the disturbances during GATE suggests that the surges in the trades may have a relationship to westward propagating pressure pulsations. If the low pressure area is well North of the equator, then the surge is often first noted in the Northeast trades. On the other hand, if the pressure perturbation is just North of the equator then the surge is first noted in the Southeast trades. These results on the relationship between the surges of the trades of the two hemispheres are especially noteworthy since the two regions centered at 0°, 30°W and 20°W, 40°W have no common data sets and are well separated from each other. Figs. 16a, b illustrate the spectra of the meridional wind and of the total stress based on the 100 days of surface wind data for the Southeast trades. Peaks in the 4 to 6 day range and around 11 day period are prominant features in their spectra.

In summary, the trade winds of the summer and the winter hemispheres show oscillation in the 3 to 6 day as well as in the 10 to 15 day periods. The 3 to 6 day period is most likely related to westward propagating African waves. The 10 to 15 day period appears to be related to a westward propagating wave. An illustration of this type of wave is shown on an x-t diagram in Fig. 17. Here we have taken the meridional surface wind, V, for the 100 days of GATE at 20°N and subjected it to a band pass filter which has a maximum response of around 15 days and a near zero response below 10 days as

well as above 20 days. The region for $V < 0$ is shaded in this illustration. We find a well-defined westward propagating wave for most of the 100 day period. The wavelength of this wave $\simeq 40^{\circ}$ long, and its speed $\simeq 3^{\circ}$ long/day. This wave in the 10-15 day period was also noted from the data sets of the meridional wind at 850 mb. We find very little vertical tilt of this wave in the lower troposphere.

7. Concluding Remarks

The future determination of the wind stress over the global oceans will depend more and more on observations obtained via remote sensing from satellites. One of the proposed satellites, called SEASAT, makes use of a scatterometer to determine the surface stresses. This satellite was launched during 1978 and produced data of high quality for only a 90 day period prior to its failure. The geostationary satellites provide cloud wind data which are presently being used to define the motion field at around the 1 km height above sea level. The present paper is an effort to include this important data set for the analysis and determination of surface winds as well as the stresses. The proposed technique allows for a turning of wind with height by incorporating this information via a successive correction in the wind analysis. The proposed method is calibrated against the GATE research ship surface observations. The potential of the proposed method lies in its further use during FGGE (The First GARP Global Experiment) when 5 geostationary satellites along with 50 research ships and 1000 merchant ships are expected to provide a composite observing system. This data set should provide the possibility for determination of detailed surface motion field as well as the wind

stresses and their variability over global oceans.

The present study, although somewhat limited in scope, i.e. limited domain and short period of 100 days, has nevertheless enabled us to define these fields with some degree of accuracy that was not possible previously. The important results of the present study include i) a technique for incorporating the low cloud motion vectors in the surface wind analysis, ii) mean motion field as well as the mean stresses over the tropical Atlantic ocean during the northern summer, iii) the variability of the motion field and the stresses on two dominant time scales: 3 to 6 days and 10 to 15 days, both of which are identified as westward propagating modes. The former is here identified with the passage of African waves; while the latter, whose scale is on the order of 40° longitude with a speed of propagation of about 2.7° longitude/day, is not presently understood. Its importance however in oceanographic problems has appeared in many recent studies.

Acknowledgements

This work was supported by the following grants: i) Office of Naval Research Grant No: ONR-N00014-75-C-0877 to the Department of Oceanography, ii) National Science Foundation ATM75-18945 to the Department of Meteorology. The computer facilities of the Florida State University (CYBER 73) and at the National Center for Atmospheric Research (CDC 7600) provided the computational support.

REFERENCES

Brummer, B., F. Ostaposs, and H. Schmidt, 1973: The aerological measurements during ATEX. NOAA Technical Report. Parts I, II and III, published by the National Oceanic and Atmospheric Administration. Available from the U.S. Government Printing Office.

Businer, J. and W. Seguin, 1977: Sea-air flows of latent and sensible heat and momentum. Proceedings of the GATE Workshop published by the National Center for Atmospheric Research, Boulder, Colorado. pp. 441-453.

Charnock, H., J.R.D. Francis and P. A. Sheppard, 1956: An investigation of wind structure in the trades. Anegada, 1953. Philosophical Transactions. A, 179-234.

Dean, G. and C. Smith, 1977: A study of synoptic and mesoscale interactions over the GATE ship network. Technical Note NCAR/TN-122 + STR. NCAR, Boulder, Colorado, pp. 1-95.

Dittmer, K., M. Gruenewald and L. Hassee, 1978: Turbulent flows in the surface layer from profile measurements during GATE. "Meteor" Forschungsergebnisse, Riehe, B.

Duing, Walter, 1968: The monsoon regime of the currents in the Indian Ocean. Technical Report., Department of Oceanography. University of Hawaii, Honolulu. pp. 1-81.

Hantel, M., 1970: Monthly charts of surface wind stress curl over the Indian Ocean. Mon. Wea. Rev., 98, 765-773.

Hellerman, S., 1967: An updated estimate of the wind stress on the world ocean. Mon. Wea. Rev., 95, 607-626.

Holland, J. Z., and E. M. Rasmusson, 1973: Measurements of the atmosphere mass, energy and momentum budgets over a 500-km square of tropical ocean. Mon. Wea. Rev., 101, 44-55.

Holopaineu, G. O., 1967: A determination of wind driven ocean circulation from the vorticity budget of the atmosphere. PAGEOPH, 67, 156-165.

Hubert, L. F., 1975: Evaluation of wind data derived from SMS-1 or characteristics of satellite wind data. Paper presented at the 9th Technical Conference on Hurricanes and Tropical Meteorology. Miami, Florida, 1-8, May 1975.

Jacobs, C. A., 1978: Observed semidiurnal fluctuations in the air-sea fluxes during GATE. Paper presented at the "GATE Symposium on Oceanography and Surface Layer Meteorology". Kiel (16 - 20, May 1978). (To be published in Deep Sea Research).

Krishnamurti, T. N., C. E. Levy and Hua-lu Pan, 1975: On simultaneous surges in the trades. J. Atmos. Sci., 32, 2367-2370.

_____, G. Van Dam, H. L. Pan, L. Hughes, R. J. Pasch, Robert McGraw, 1976a: Cloud motion vectors for GATE. Tech. Rept. No. 76-1, Department of Meteorology, Florida State University, Tallahassee, Florida. pp. 1-22.

_____, and H. N. Bhalme, 1976b: Oscillations of a monsoon system, Part 1, observational aspects. J. Atmos. Sci., 33, 1937-1954.

Miller, B. I., 1962: On the energy and momentum balance of Hurricane Helene (1958). National Hurricane Research Project Report No. 53, U.S. Weather Bureau, 19 pp.

Murakami, M., 1979: Large scale aspect of convective activity over the GATE area (submitted for publication to the Monthly Weather Review).

Ooyama, K., 1969: Numerical simulation of the life cycle of tropical cyclones. J. Atmos. Sci., 26, 3-40.

Roll, H. V., 1965: Physics of the Marine Atmosphere. New York and London. Academic Press. 1-426 (see page 160).

Tripoli, G. H., and T. N. Krishnamurti, 1975: Low level flows over the GATE area during summer 1972. Mon. Wea. Rev., 103, 197-216.

Wallace, J. M., 1971: Spectral studies of tropospheric wave disturbances in the tropical western Pacific. Rev. Geophys. S. Phys., 9, 557-612.

Wyngaard, J. C., 1975: Modelling the planetary boundary layer-extension to the stable case. Boundary Layer Meteorology, 9, 441-460.

Yanai, M., 1964: An experimental objective analysis in the tropics. Tech. Paper No. 62, Colorado State University, Fort Collins. pp. 1-34.

_____, T. Maruyama, T. Nitta and Y. Hayashi, 1968: Power spectra of large scale disturbances over the Pacific. J. Meteor. Soc. Japan, 46, 308-323.

Zangvil, A., 1975: Temporal and spatial behavior of large-scale disturbances in tropical cloudiness deduced from satellite brightness data. Mon. Wea. Rev., 103, 904-920.

Table 1. LIST OF USEFUL SYMBOLS

SYMBOL	MEANING OF SYMBOL
D_{sij}	Surface wind direction at a point i,j.
D_{cij}, D_c	Direction of cloud wind at a point i,j.
δ_{ij}	Turning angle at a point i,j.
(overbar)	Mean value within a subdomain.
S_{sij}	Surface wind speed at a point i,j.
S_{cij}, S_c	Speed of cloud wind at a piont i,j.
u_{cs}, v_{cs}	Zonal and meridional components of cloud wind relocated at the surface level.
u_g	Geostrophic wind.
z_a	Height of Anemometer level.
z_o	Roughness length.
u_*	Friction velocity.
L	Monin-Obukhov length.
κ	Von Karman constant
f	Coriolis parameter.
h	Height of planetary boundary layer.
α_o	Mean turning of wind with height in the planetary boundary layer.
θ_o	Angle between surface pressure gradient and the east.
C_D	Drag coefficient.
τ_x, τ_y	Components of wind stress.
C_{WS}	Curl of the wind stress.

Fig. 1. The distribution of GATE ships (phase III) over the Atlantic Ocean is shown here. Circle with cross indicates B-scale radar ships, square with circle within indicates A/B scale ships, dark square within a square are the A-scale ships, circle denotes B-scale ship positions.

Fig. 2. The distribution of merchant ships on a typical day.

Fig. 3. A sample distribution of low cloud motion vectors over the Atlantic ocean. (Courtesy of Fujita).

Fig. 4a. (top) Mean streamlines and isotachs (mps) for Phase III (12Z) based on the proposed analysis scheme.

Fig. 4b. (middle) Mean streamlines for phase III (12Z) from Dean and Smith.

Fig. 4c. Final surface analysis at the surface for a typical day. wind barbs (knots). Data from a mix of platforms is shown here.

Fig. 5a. (top) Mean surface streamlines and isotachs (mps) for the 100 days of GATE.

Fig. 5b. (bottom) Mean surface streamlines and isotachs (mps) for the IIIrd phase of GATE.

Fig. 6a. (top) Mean 850 mb streamlines and isotachs (mps) for the 100 days of GATE.

Fig. 6b. (bottom) Mean 850 mb streamlines and isotachs (mps) for the IIIrd phase of GATE.

Fig. 7. Mean turning angle (in degrees) of wind between the surface and the low cloud wind level. (Note: low cloud wind level is not necessarily the top of the friction layer). Positive values: Backing; negative values: Veering.

Fig. 8a. (top) 100 day mean surface field of the meridional stress (dynes/cm^2).

Fig. 8b. (bottom) Phase III mean field surface of the meridional stress (dynes/cm^2).

Fig. 9a. (top) 100 day mean field of the surface zonal stress. (dynes/cm^2).

Fig. 9b. (bottom) Phase III mean field of the surface zonal stress (dynes/cm^2).

Fig. 10a. (top) 100 day mean field of the surface total stress (dynes/cm^2).

Fig. 10b. (bottom) Phase III mean field of the surface total stress (dynes/cm^2).

Fig. 11a. (top) and Fig. 11b. (bottom) Zonal and meridional components of the wind stress (dynes/cm^2) based on Hellerman's study.

Fig. 12a. (top) 100 day mean field of the surface wind stress curl. Units: x10^{-10} dynes/cm^3.

Fig. 12b. (bottom) Phase III mean field of the surface wind stress curl. Units: x10^{-10} dynes/cm^3.

Fig. 13a. (top) Variability of the surface zonal wind (mps) of the north-east trades during the 100 days of GATE.

Fig. 13b. (bottom) Spectral analysis of the surface zonal wind for N.E. trades. Plots show the product of power times the frequency plotted against the log of frequency.

Fig. 14a. (top) Spectral analysis of the surface meridional wind for the N.E. trades. Plots show the product of power times the frequency plotted against the log of the frequency.

Fig. 14b. (bottom) Spectral analysis of the total stress.

Fig. 15a. Variability of the zonal wind (mps) during the 100 days of GATE for the southeast trades.

Fig. 15b. Spectral analysis of the zonal wind for the southeast trades.

Fig. 16a. Spectral analysis of the meridional wind for the southeast trades.

Fig. 16b. Spectral analysis of the total wind stress for the southeast trades.

Fig. 17. An x-t diagram at 20^{O}N for the 10 to 20 day mode of the meridional wind. The shaded area denotes $v < 0$, while the unshaded area represents southerly motion.

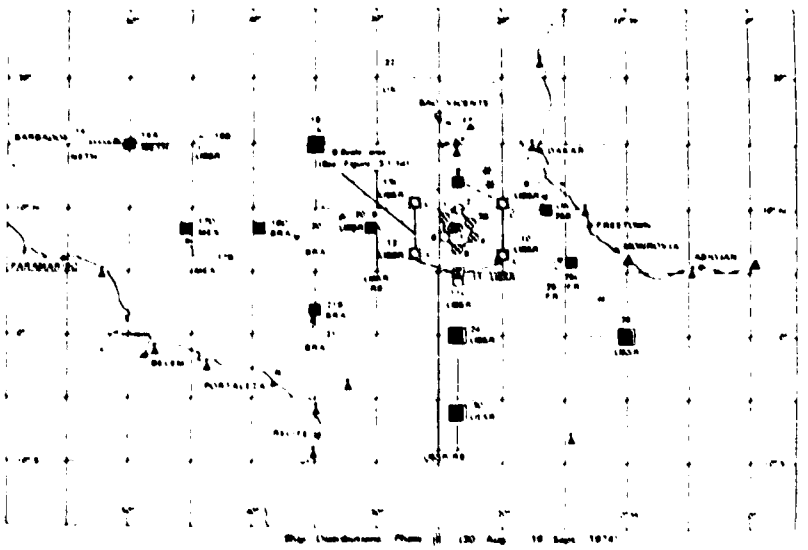

Fig. 1. The distribution of GATE ships (phase III) over the Atlantic Ocean is shown here. Circle with cross indicates B-scale radar ships, square with circle within indicates A/B scale ships, dark square within a square are the A-scale ships, circle denotes B-scale ship positions.

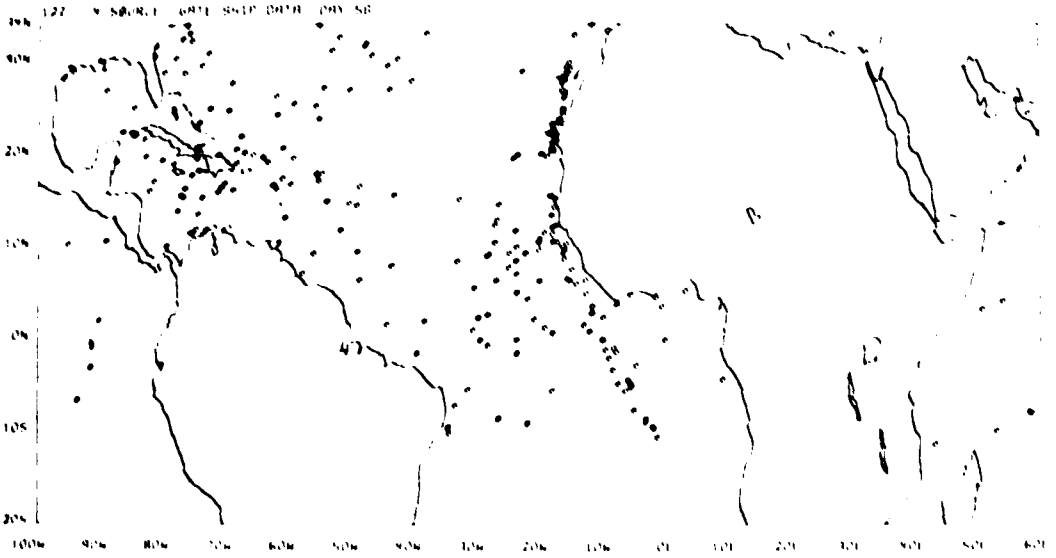

Fig. 2. The distribution of merchant ships on a typical day.

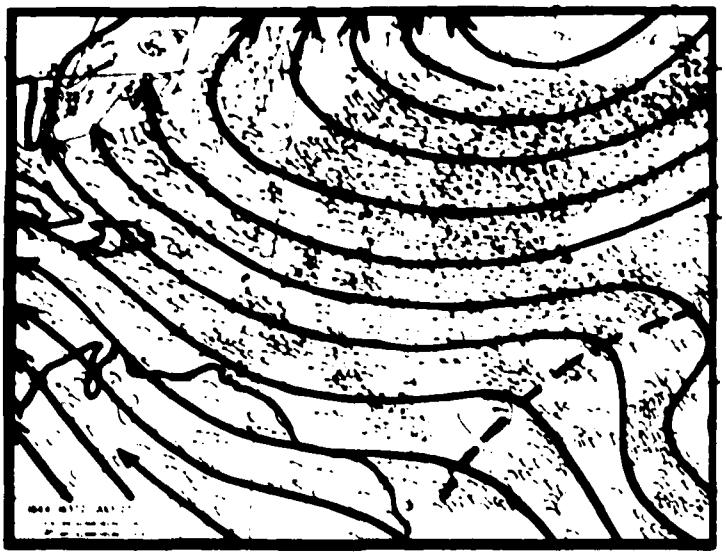

Fig. 3. A sample distribution of low cloud motion vectors over the Atlantic ocean. (Courtesy of Fujita).

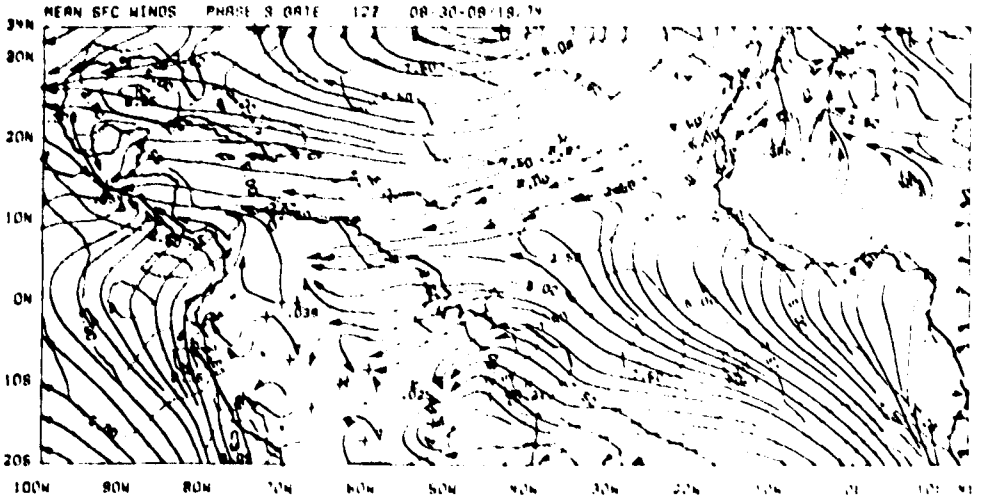

Fig. 4a. Mean streamlines and isotachs (mps) for Phase III (123) based on the proposed analysis scheme.

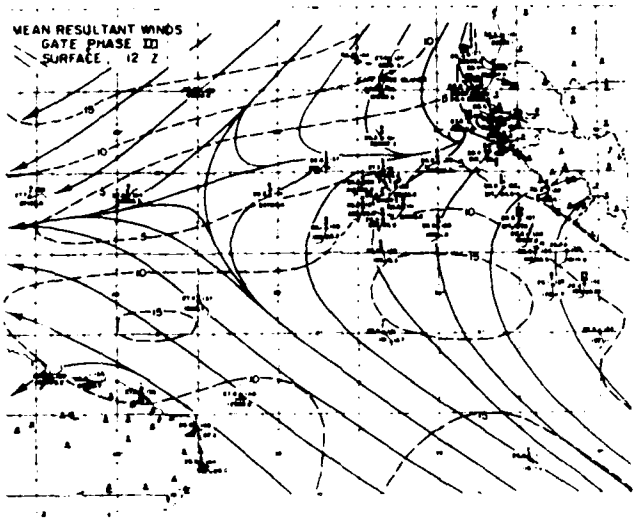

Fig. 4b. Mean streamlines for phase III (12Z) from Dean and Smith.

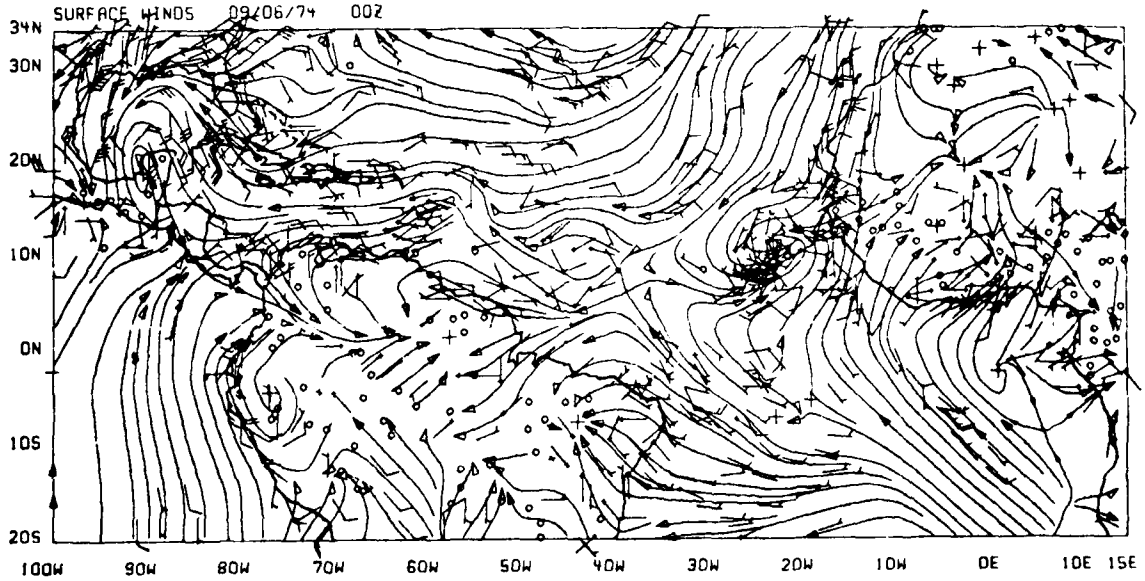

Fig. 4c. Final surface analysis at the surface for a typical day. wind barbs (knots). Data from a mix of platforms is shown here.

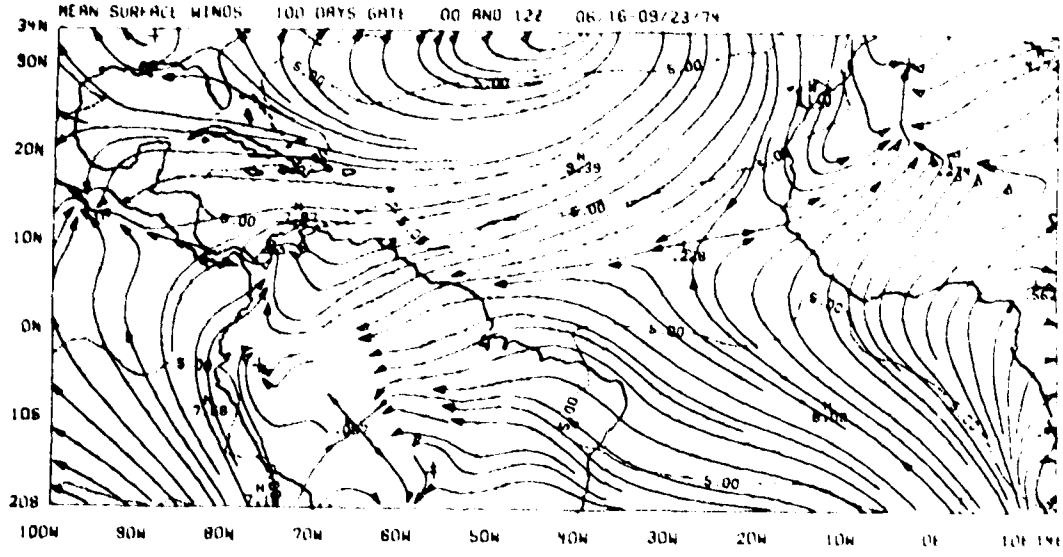

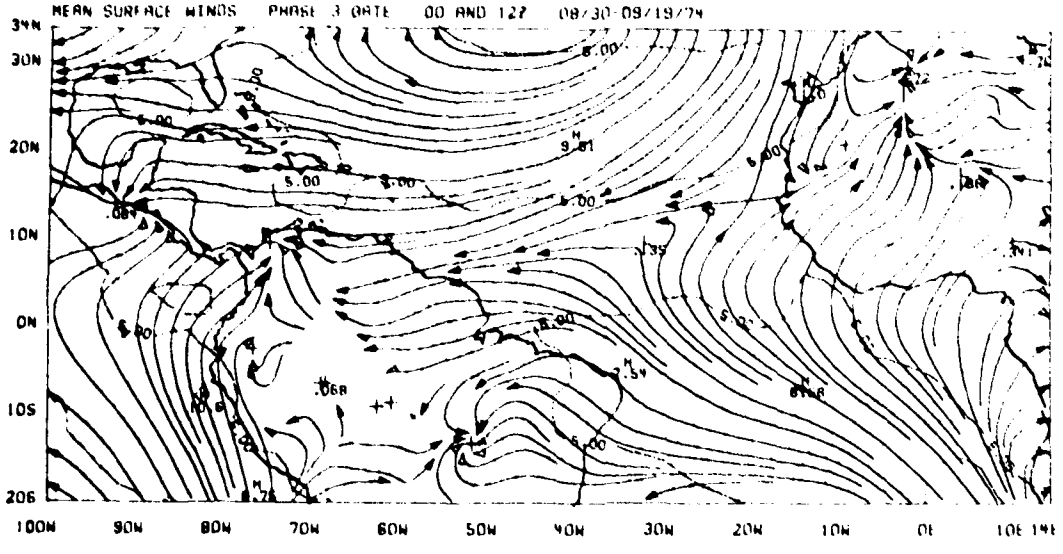

Fig. 5a. Mean surface streamlines and isotachs (mps) for the 100 days of (top) GATE.

Fig. 5b. Mean surface streamlines and isotachs (mps) for the IIIrd phase (bottom) of GATE.

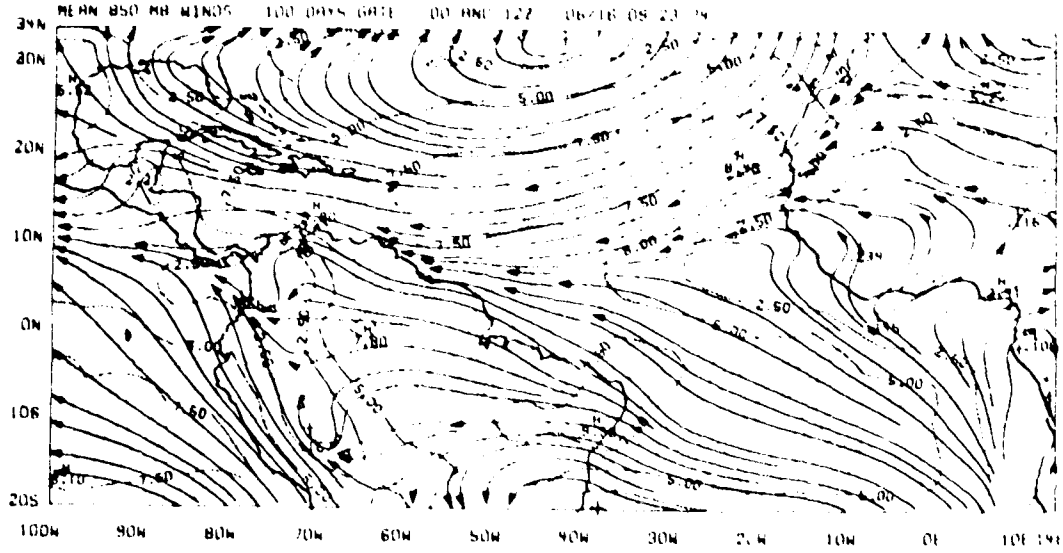

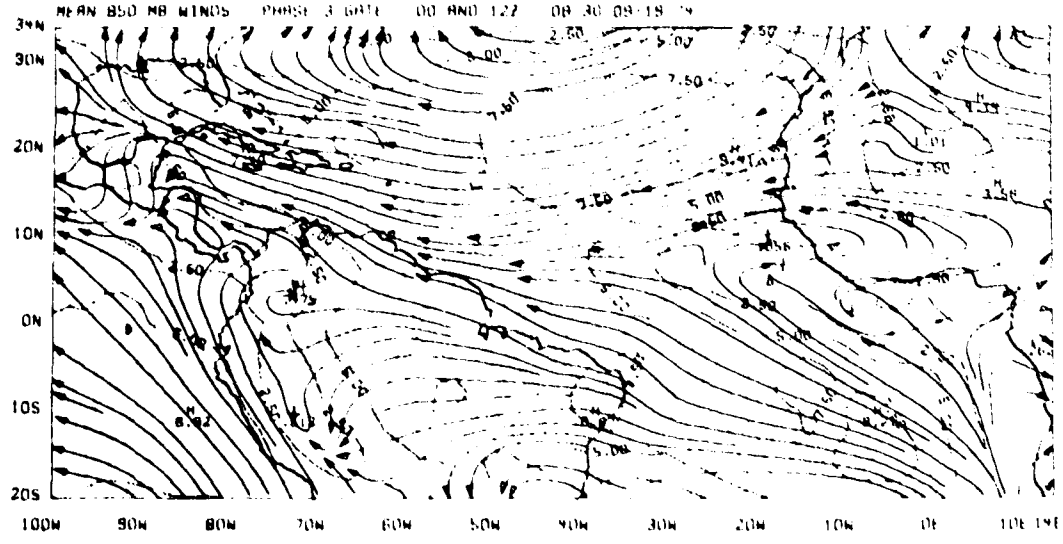

Fig. 6a. Mean 850 mb streamlines and isotachs (mps) for the 100 days of (top) GATE.

Fig. 6b. Mean 850 mb streamlines and isotachs (mps) for the IIIrd phase (bottom) of GATE.

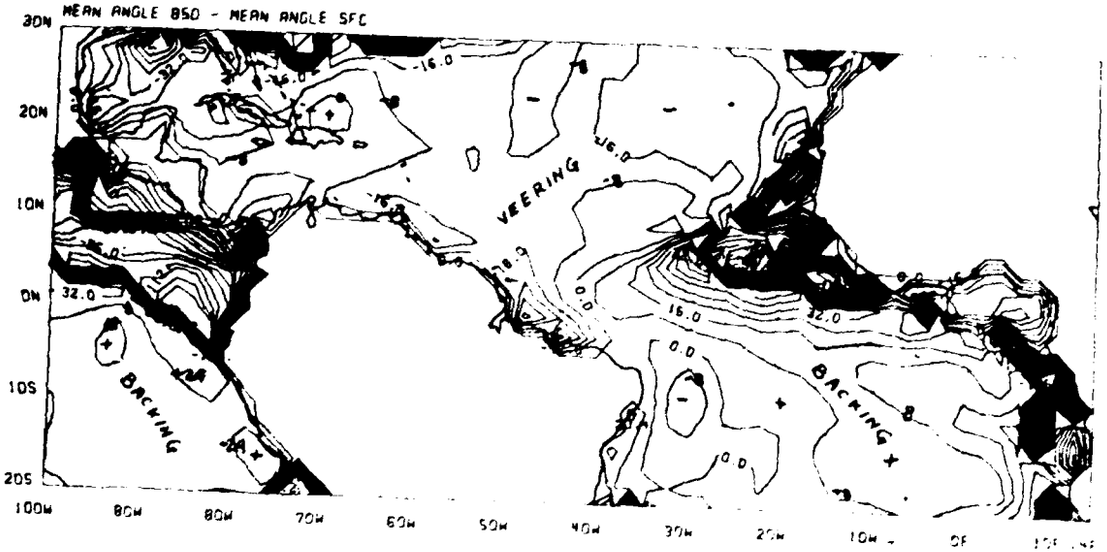

Fig. 7. Mean turning angle (in degrees) of wind between the surface and the low cloud wind level. (Note: low cloud wind level is not necessarily the top of the friction layer). Positive values: Backing; negative values: Veering.

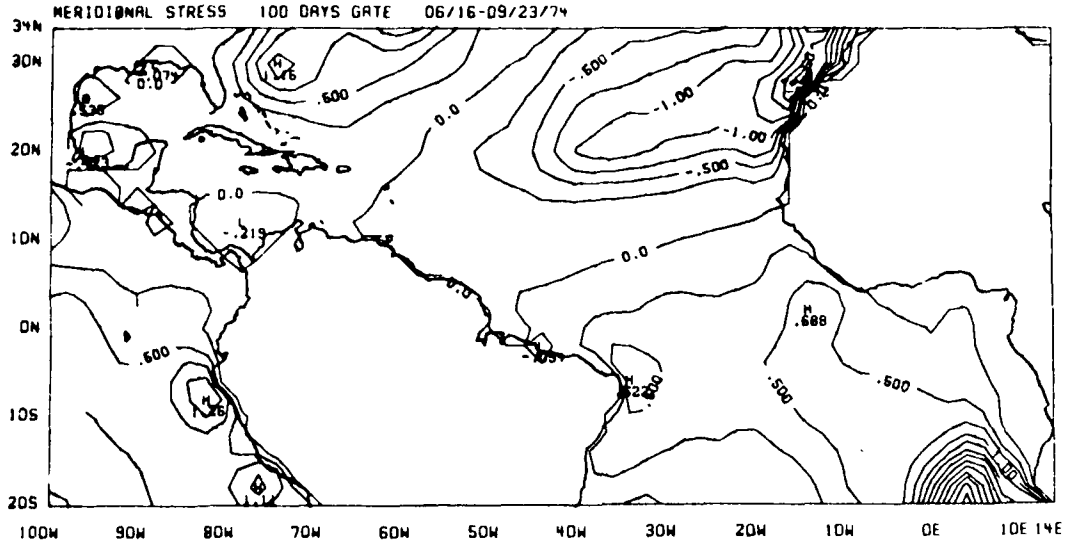

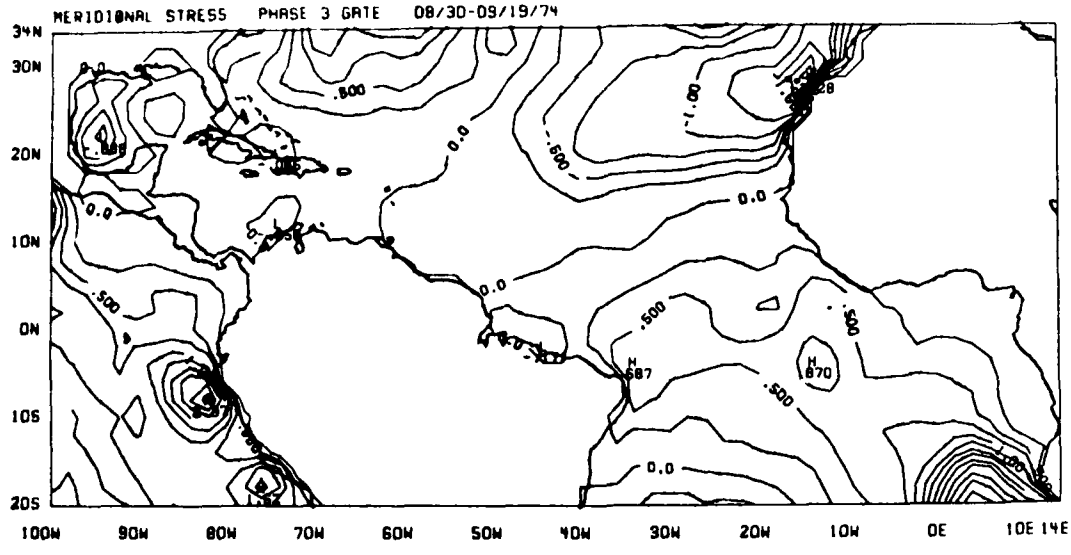

Fig. 8a. 100 day mean surface field of the meridional stress (dynes/cm^2). (top)

Fig. 8b. Phase III mean field surface of the meridional stress (dynes/cm^2). (bottom)

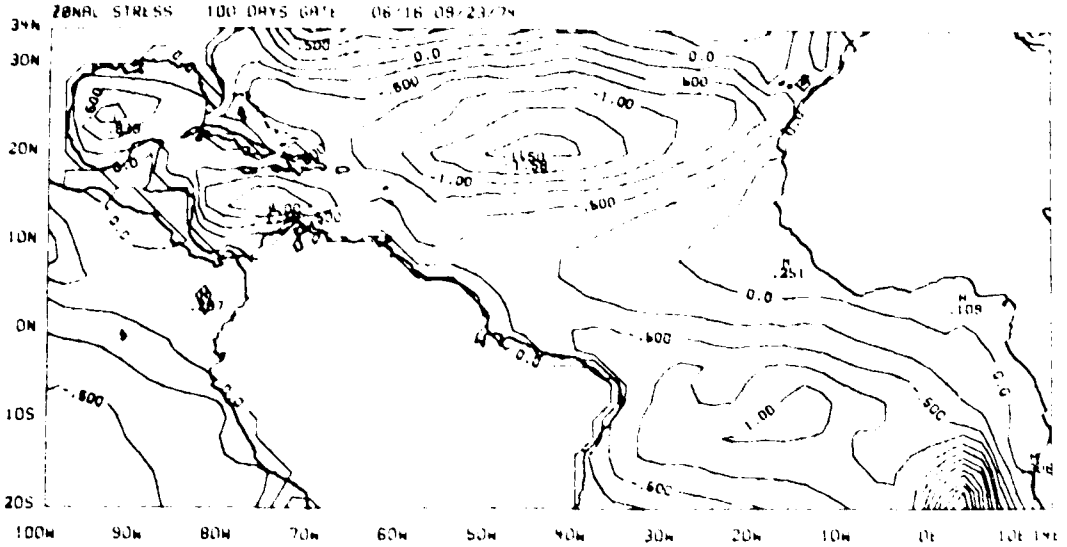

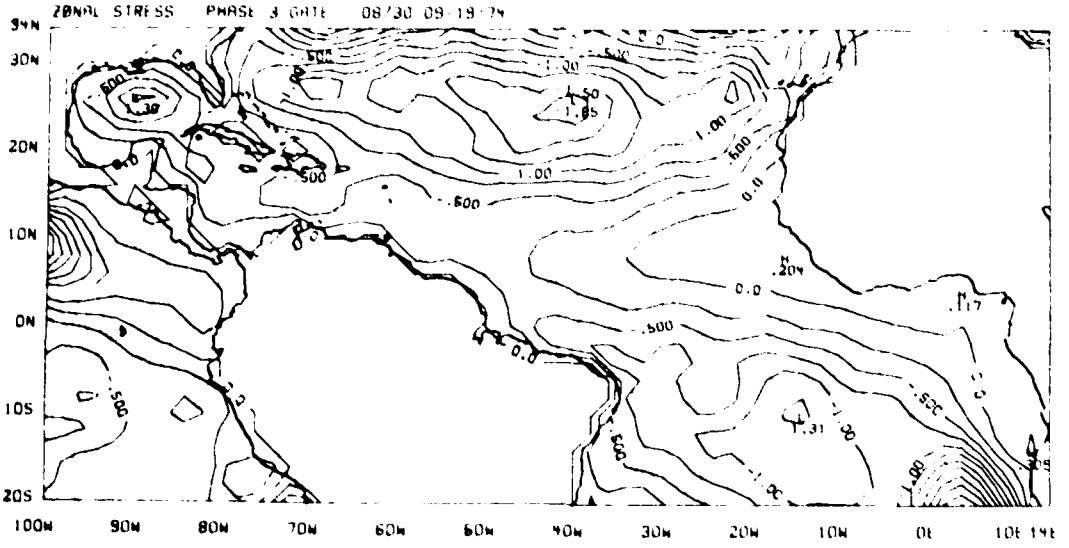

Fig. 9a. 100 day mean field of the surface zonal stress. (dynes/cm^2). (top)

Fig. 9b. Phase III mean field of the surface zonal stress (dynes/cm^2). (bottom)

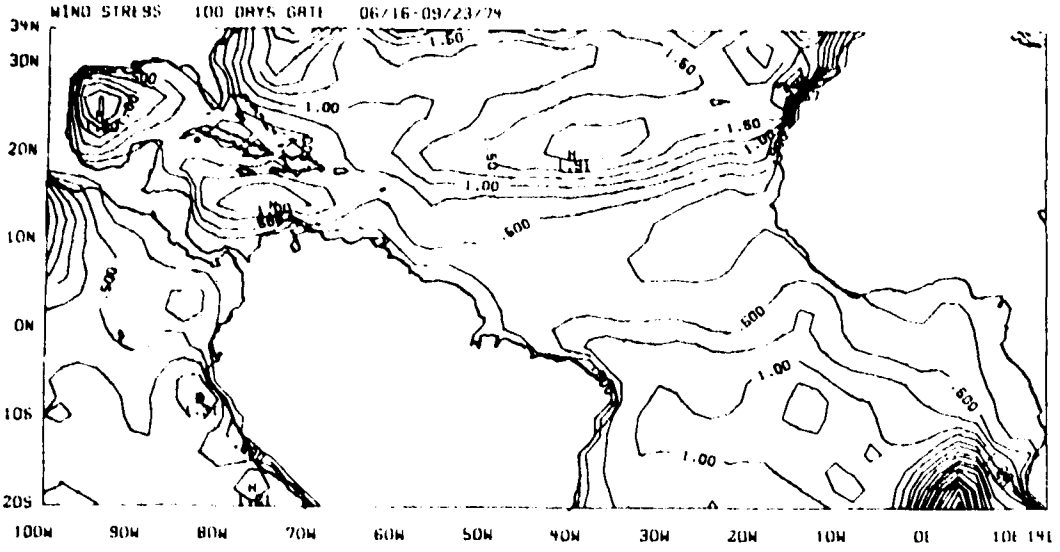

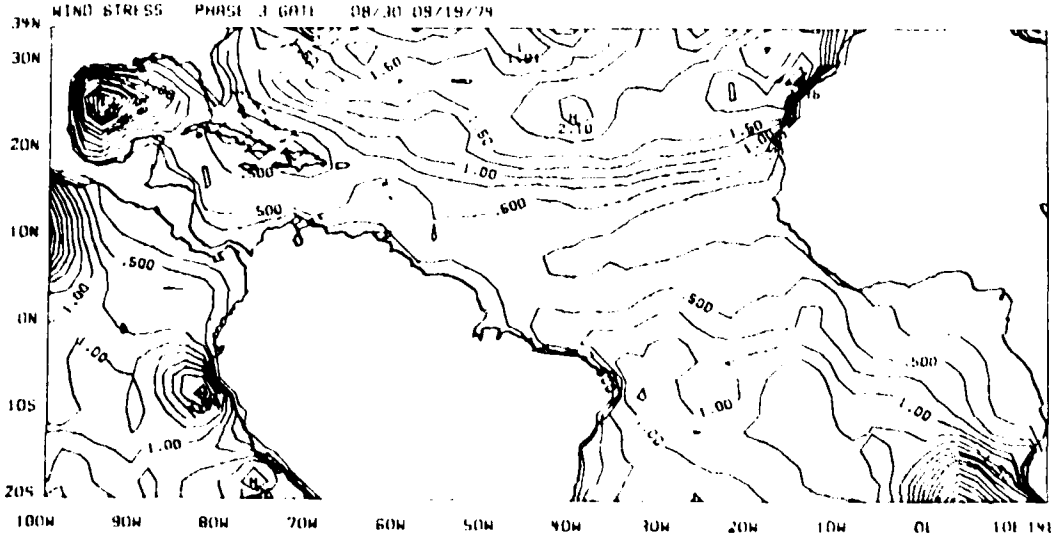

Fig. 10a. 100 day mean field of the surface total stress (dynes/cm^2). (top)

Fig. 10b. Phase III mean field of the surface total stress (dynes/cm^2). (bottom)

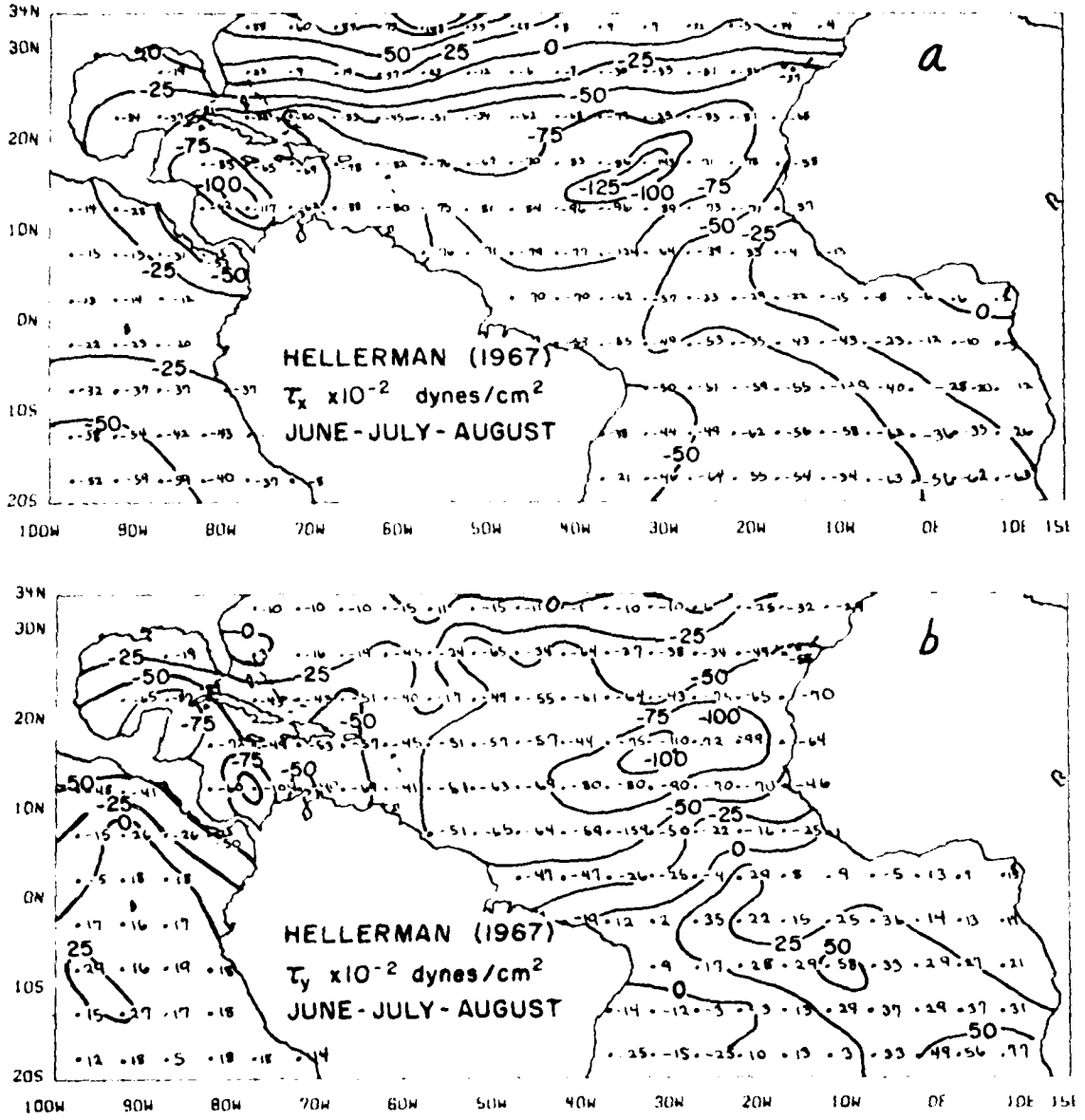

Fig. (*11a,b*). Zonal and meridional components of wind stress (dynes/cm^2) x 10^{-2} based on Hellerman's study.

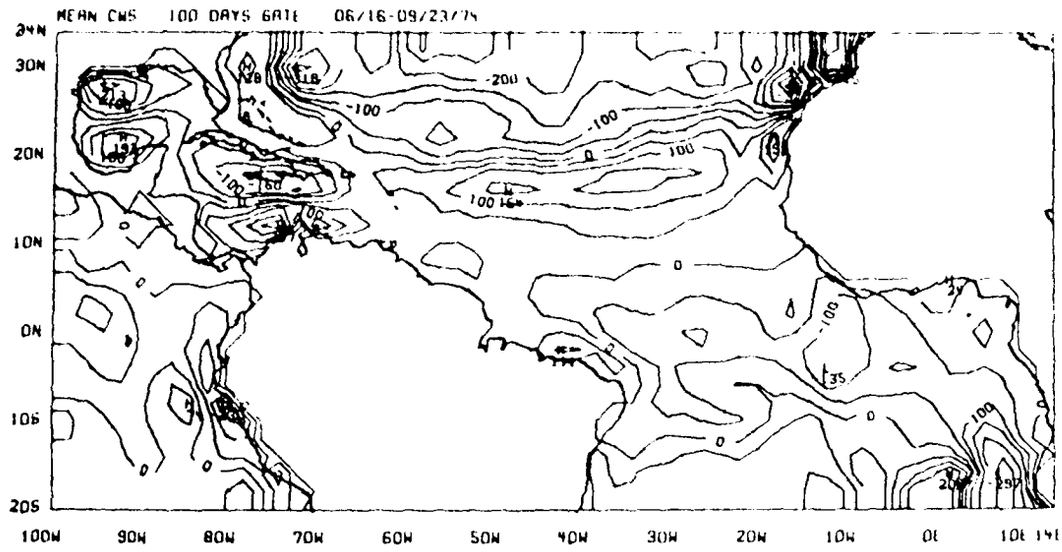

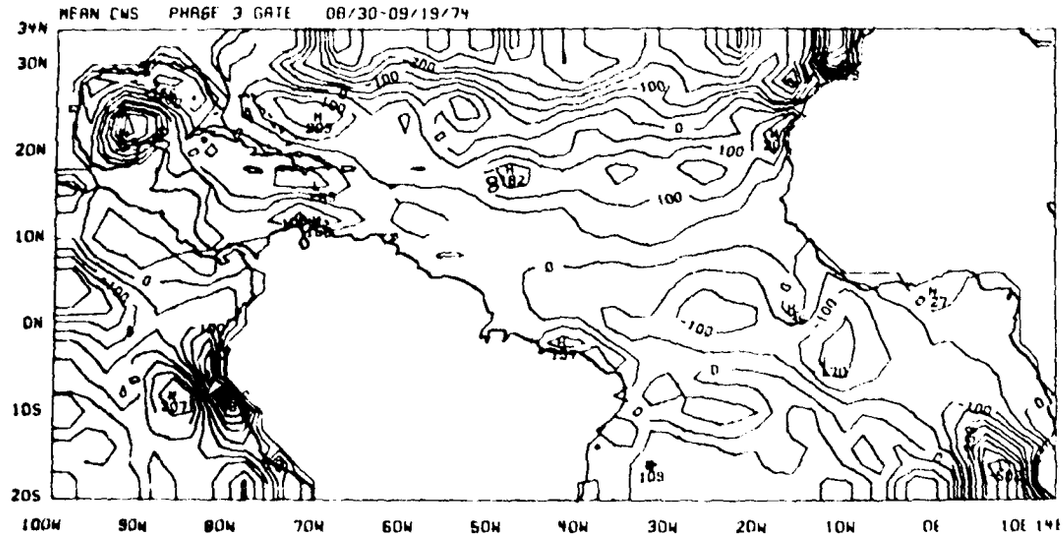

Fig. 12a. 100 day mean field of the surface wind stress curl.
(top) Units: x 10^{-10} dynes/cm^3

Fig. 12b. Phase III mean field of the surface wind stress curl.
(bottom) Units: x 10^{-10} dynes/cm^3

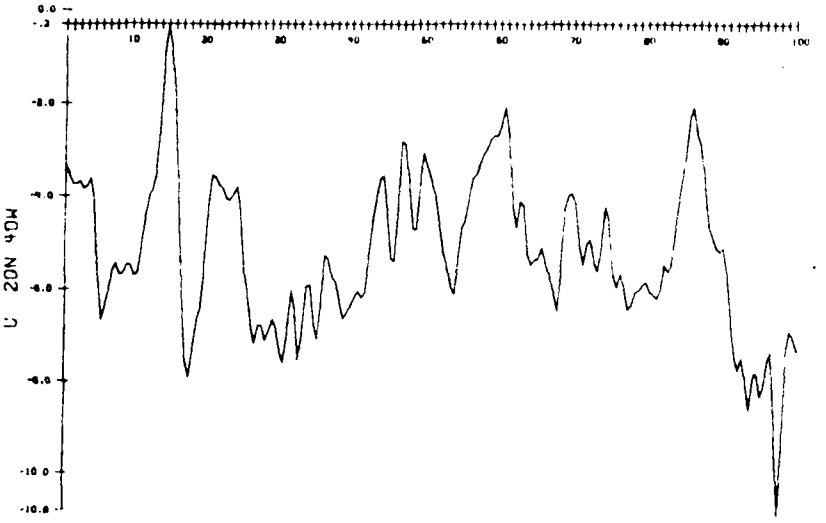

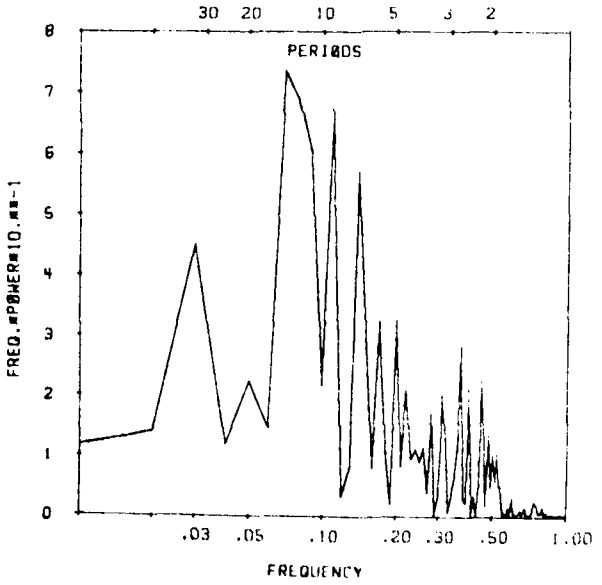

Fig. 13a. (top) Variability of the surface zonal wind (mps) of the northeast trades during the 100 days of GATE.

Fig. 13b. (bottom) Spectral analysis of the surface zonal wind for N.E. trades. Plots show the product of power times the frequency plotted against the log of frequency.

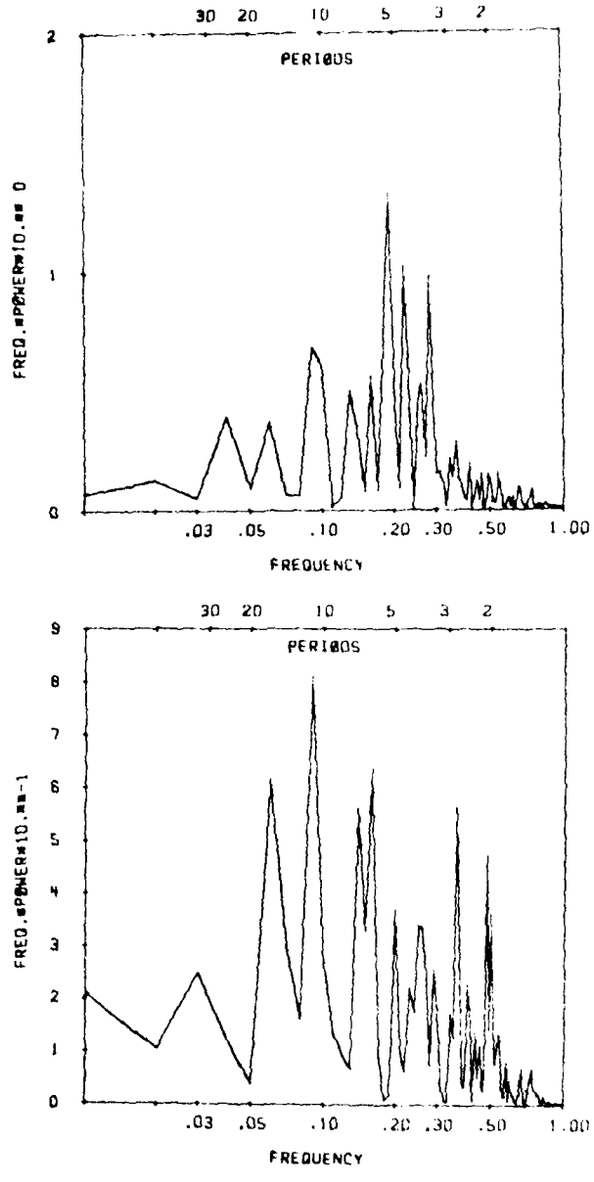

Fig. 14a. (top) Spectral analysis of the surface meridional wind for the N.E. trades. Plots show the product of power times the frequency plotted against the log of the frequency.

Fig. 14b. (bottom) Spectral analysis of the total stress.

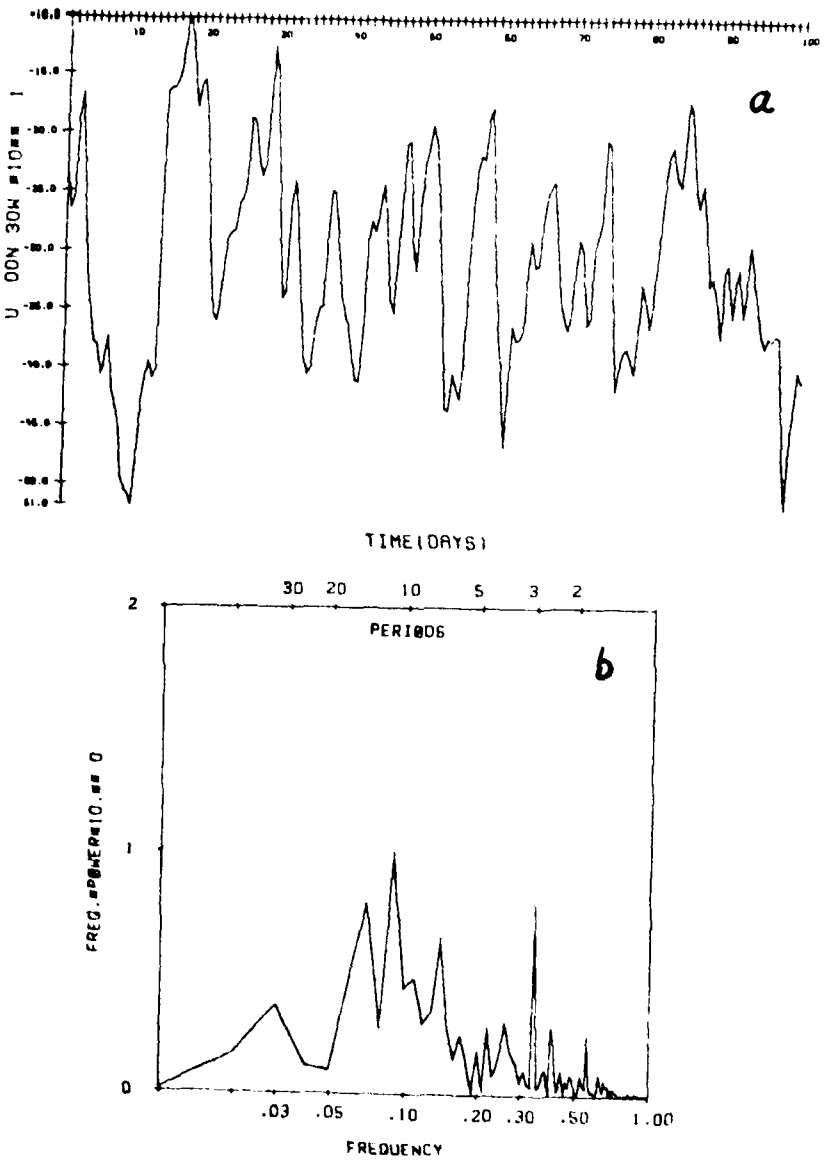

Fig. 15a. Variability of the zonal wind (mps) during the 100 days of GATE for the southeast trades.

Fig. 15b. Spectral analysis of the zonal wind for the southeast trades.

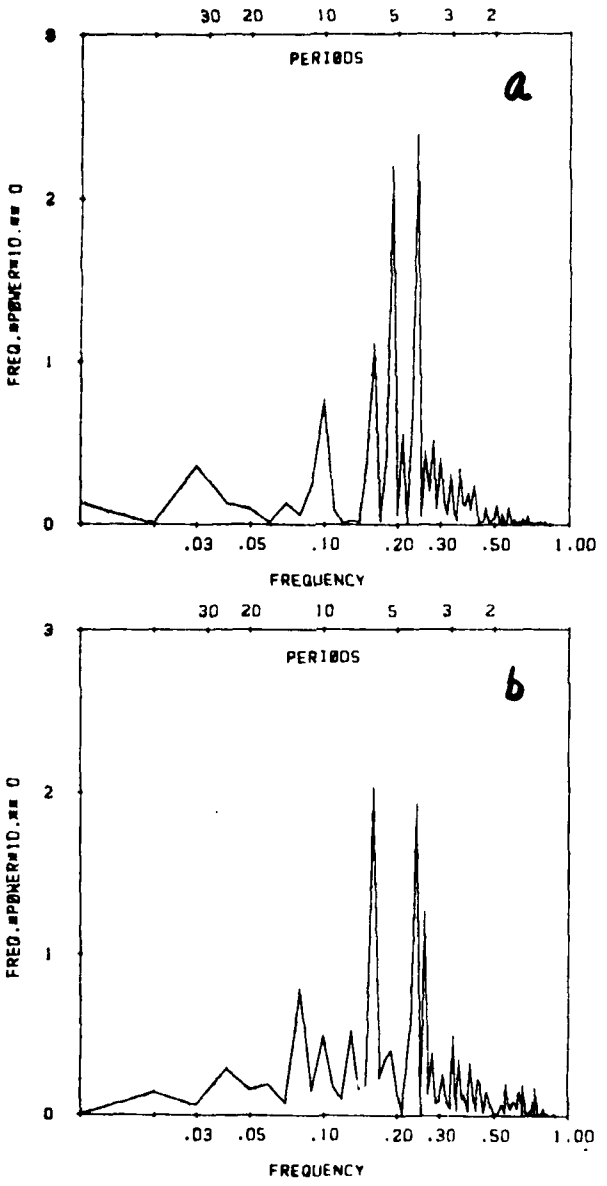

Fig. 16a. Spectral analysis of the meridional wind for the southeast trades.

Fig. 16b. Spectral analysis of the total wind stress for the southeast trades.

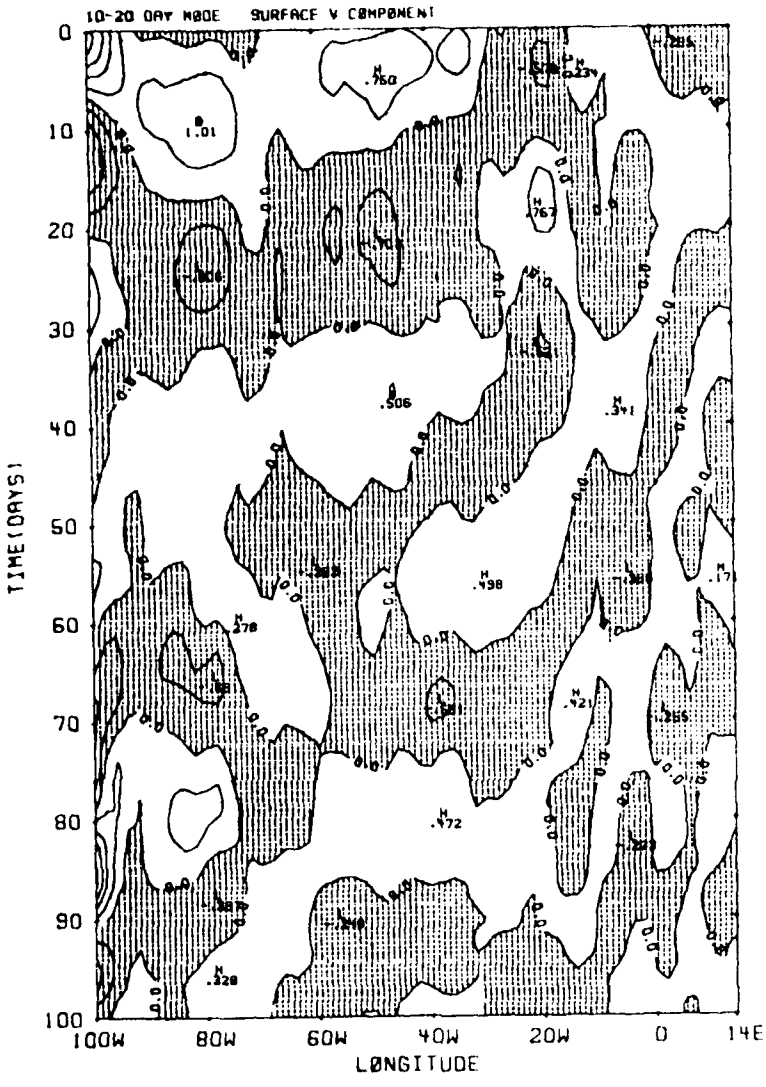

Fig. 17. An x-t diagram at 20°N for the 10 to 20 day mode of the meridional wind. The shaded area denotes $v < 0$, while the unshaded area represents southerly motion.

SECURITY CLASSIFICATION OF THIS PAGE (When Data Entered)

REPORT DOCUMENTATION PAGE

READ INSTRUCTIONS BEFORE COMPLETING FORM

1. REPORT NUMBER: (9) Technical Report, No. 16	2. GOVT ACCESSION NO.: (14) 78-6,TR-16
3. RECIPIENT'S CATALOG NUMBER	
4. TITLE (and Subtitle): SURFACE METEOROLOGY OVER THE GATE A-SCALE	5. TYPE OF REPORT & PERIOD COVERED
	6. PERFORMING ORG. REPORT NUMBER
7. AUTHOR(s): T.N. Krishnamurti# [redacted] Ruby Krishnamurti*	8. CONTRACT OR GRANT NUMBER(s): (15) [redacted] N00014-75-C-0877
9. PERFORMING ORGANIZATION NAME AND ADDRESS: Department of Meteorology# and Oceanography* Florida State University Tallahassee, Florida 32306	10. PROGRAM ELEMENT, PROJECT, TASK AREA & WORK UNIT NUMBERS: 12, 62
11. CONTROLLING OFFICE NAME AND ADDRESS: (11)	12. REPORT DATE: Nov[redacted]78
	13. NUMBER OF PAGES: 45
14. MONITORING AGENCY NAME & ADDRESS (if different from Controlling Office): Office of Naval Research Fluid Dynamics	15. SECURITY CLASS. (of this report)
	15a. DECLASSIFICATION/DOWNGRADING SCHEDULE

16. DISTRIBUTION STATEMENT (of this Report)

This is a technical report to the Office of Naval Research under Contract N-00014-75-C-0877 [redacted] Reproduction in whole or in part is permitted for US Gov't.

17. DISTRIBUTION STATEMENT (of the abstract entered in Block 20, if different from Report)

18. SUPPLEMENTARY NOTES

19. KEY WORDS (Continue on reverse side if necessary and identify by block number)

20. ABSTRACT (Continue on reverse side if necessary and identify by block number)

A method of analysis for the surface motion field based on a mix of obversations from research ships, merchant ships and low cloud motion vectors from geostationary satellites is proposed in this paper. The proposed scheme permits a turning of wind with height between the cloud wind level and the surface. This turning is incorporated via a successive correction procedure which enables us to fully utilize the low-cloud winds. The method does not depend on a predetermined theory. The analysis of the surface wind field is

(cond on next page)

DD FORM 1 JAN 73 1473 EDITION OF 1 NOV 65 IS OBSOLETE S/N 0102-014-6601

SECURITY CLASSIFICATION OF THIS PAGE (When Data Entered)

401 468

(cond. from previous page · Block 20)

carried out for the 100 days of the GARP ATLANTIC TROPICAL EXPERIMENT (GATE) for two observation periods per day (00Z, 12Z) over a wide domain.

This paper illustrates (i) time averaged geometry of the motion field during GATE, and ~~ii~~ (ii) time averaged fields of the zonal and the meridional stresses as well as of the curl of the wind stress. Finally, we examine the spectral analysis of the motion field and the stresses over the trade wind belts of the summer and winter hemisphere. Our study emphasizes the importance of two modes of oscillation, one around 3 to 6 days and the other around 10 to 15 days. While the former is identified with African waves, the scale and speed of propagation of the latter is determined from x-t diagrams and is identified as a westward propagating wave, whose scale is of the order of 40^{o} longitude and speed of propagation is around 3^{o} longitude/day. This study emphasizes the possible usefulness of this approach during the GARP Global Experiment when a global coverage from geostationary satellites is expected.